Tellus SERIES A DYANAMIC METEOROLOGY AND OCEANOGRAPHY
PUBLISHED BY THE INTERNATIONAL METEOROLOGICAL INSTITUTE IN STOCKHOLM

Observations of internal waves generated by an anticyclonic eddy: a case study in the ice edge region of the Greenland Sea

By O.M. JOHANNESSEN[1]*, S. SANDVEN[2], I.P. CHUNCHUZOV[3], and R.A. SHUCHMAN[4], [1]*Nansen Scientific Society, Bergen, Norway;* [2]*Nansen Environmental and Remote Sensing Center, Bergen, Norway;* [3]*Obukhov Institute of Atmospheric Physics, Moscow, Russia;* [4]*Michigan Tech Research Institute, Ann Arbor, MI, USA*

(Manuscript received 06 September 2018; in final form 01 August 2019)

ABSTRACT

Internal waves in the ocean play an important role in turbulence generation due to wave-breaking processes and mixing of the ocean. Airborne radar images of internal waves and ocean eddies north of Svalbard suggested that ocean eddies could generate internal waves. Here, we test this hypothesis using data from a dedicated internal wave experiment in the Greenland Sea. Internal waves with dominant frequencies of 1–3 cycles per hour and amplitudes up to 15 m were observed using three thermistor chains suspended from a drifting array conveniently placed on the ice in a triangle with sides of several km. Analysis shows that internal waves propagated westwards with a speed of about 0.2 m/s and wavelength of 0.4–1.0 km, away from an anticyclonic ocean eddy located just east of the array. This was consistent with the remote-sensing observations of internal waves whose surface signature was imaged by an airborne radar in the western part of this eddy, and with theories that eddies and vortexes can directly generate internal waves. This case study supports our hypothesis that ocean eddies can be the direct sources of internal waves reported here for the first time and not only enhancing the local internal wave field by draining energy from the eddies, as studied previously. The present challenge is to explore the role of eddies as a new source in generating internal waves in the global ocean.

Keywords: internal waves; ocean eddies; Greenland Sea

1. Introduction

Internal waves in the World Ocean are a well-known phenomenon important for mixing and turbulence generation in the ocean. When breaking, they cause vertical fluxes of heat, salt and momentum (Munk, 1981). As to the generation of internal waves, there are several sources, such as tidal, wind and flow over topography (Miropolsky, 2001; Alford, 2003). Some of the mechanisms of generation of internal waves remain obscure including the mechanisms of eddy dissipation in a non-balanced flow (Wunsch and Ferrari, 2004), although recent theoretical studies attempt to clarify this (Molemaker et al., 2010; Barkan et al., 2017). However, so far no observations have shown that eddies in the ocean can be the direct source for generation of internal waves, although recent observational studies show that the local internal wave field can be enhanced by draining energy from eddies (Clément et al., 2016). Previously, it was also shown that interaction of surface barotropic tides with the baroclinic eddy field could produce internal tides (Krauss, 1999).

Our aim in this paper is an attempt to show from observations that an eddy can be the direct source of generating internal waves. This hypothesis originated from interpretation of airborne radar images obtained during the NORSEX 79 Experiment (Sandven and Johannessen, 1987) and MIZEX 84 Experiment (Johannessen et al., 1986) both north of Svalbard, which suggested that ocean eddies could generate internal waves. In particular, a Synthetic Aperture Radar (SAR) image in Sandven and Johannessen (1987) indicated a small eddy with a scale of 5 km where internal waves with wavelengths of few hundred meters up to 1000 m propagated radially out from the centre of the eddy all around the eddy, most strongly

*Corresponding author. e-mail: ola.johannessen@nansenscientificsociety.no

Citation: Tellus A: 2019, **71**, 1652881, https://doi.org/10.1080/16000870.2019.1652881

towards the north-north-easterly direction towards the ice edge, which was located 12 km away from the eddy centre. These observations motivated a dedicated internal wave experiment as a part of the MIZEX 87 program (MIZEX '87 Group, 1989) in winter 1987 along the ice edge in the Greenland Sea, a region with abundant ocean eddies (Johannessen et al., 1987a, 1994). Here, based on new analysis of legacy data from MIZEX 87, we test this hypothesis and show that an anticyclonic eddy could directly generate internal waves with dominant frequencies of 1–3 cycles per hour (cph) relative to a drifting array of thermistors, and with amplitude up to 15 m.

Before describing our experiment, we will review a theoretical model for the generation of internal waves by eddies (or vortexes as called below) developed by Plougonven and Zeitlin (2002). The generation mechanism proposed is in many ways analogous to the well-known nonlinear mechanism of sound generation suggested first by Lighthill (1952), according to which the non-stationary vortex motions are sources of sound waves in a compressible medium. The non-stationarity of the vortex motion and its nonlinearity also play a significant role in the generation of internal waves in a stable stratified medium.

Plougonven and Zeitlin (2002) considered generation of internal waves by a localized pancake-like vortex of elliptical shape with a given potential vorticity. Inside the vortex, the velocity field obeys the Euler equations of stratified fluid motion in the Boussinesq approximation (when the influence of compressibility of the medium can be neglected) is purely horizontal in the first approximation over the small Froude number $\mathrm{Fr} = \mathrm{U/NL} \ll 1$, which is the ratio of the buoyancy period N to the time scale L/U of advection of the medium inside the vortex, where U is the characteristic horizontal velocity and L is the horizontal scale of the vortex. In this approximation, the vertical velocity is zero, and the advective component of acceleration is caused by the horizontal pressure gradient in accordance with Euler's equation of motion. The vertical pressure gradient is balanced by buoyancy forces, so isopycnals inside the vortex are horizontal making the vertical density gradient steeper. The buoyancy forces, being also non-stationary in the first approximation, cause temporary variations in the vertical velocity in the next approximation over the Froude number, and hence temporary variation of the horizontal velocity. This means that the nonlinearity of the vortex motion removes it from the state of quasistatic and cyclostrophic equilibrium, which is accompanied by the emission of internal waves. Thus, the mechanism of generation of internal waves is associated with the temporal pressure variations that occur inside a non-stationary localized vortex and propagate from it in the form of internal waves (Plougonven and Zeitlin, 2002). The fluxes of energy and angular momentum carried by outgoing internal waves have a backreaction to the vortex motion and its evolution over time.

From the model of generation of internal waves described above, it can be assumed that the time dependence of the motion inside the vortex determines the frequency range in which the energy of the internal waves is generated by the vortex. However, the nonlinearity of the fluid motion equation and, in particular, the advective nonlinearity lead to non-resonant and resonant interaction between emitted internal waves (Phillips, 1967; Pinkel, 2008), and between waves and horizontal vortex motions of different scales that always occur in stratified medium (Lelong and Riley, 1991). Such interactions, in turn, cause nonlinear diffusion of internal wave energy over the entire frequency–wavenumber space and lead to the formation of certain frequency and spatial spectra of velocity fluctuation and displacements of fluid parcels (Chunchuzov, 2018) At high vertical wavenumbers (i.e. for short vertical scales), these spectra of internal waves were shown to weakly depend on the initial spectra of random sources that generate these waves and vortex motions in a stably stratified medium.

To understand the mechanism of generation of internal waves by vortex motions in the ocean and the role of nonlinear interaction between internal waves and vortices in the formation of mesoscale velocity and temperature fluctuations in a wide frequency range, we need the observations to study these effects in the real ocean, which was the goal of our internal wave-eddy experiment. In this paper, we first describe the experiment (Section 2) and then the ocean structure (Section 3) including the ocean eddy field in the experimental area (Section 4), which was developing before and during internal wave observations, as described in Section 5. The analysis of the observed internal wave characteristics (periods, group velocities, azimuths of propagation) and their direct connection with the anticyclonic eddy as a source of these waves are described in Sections 6 and 7. The conclusions are presented in Section 8. In this paper, we focus on analysing the local frequencies and wavelengths for two wave crests of the entire internal wave train observed during 30–31 March 1987, which our analysis suggested was generated by an anticyclonic eddy. Actually, this wave train contains a wide range of frequencies between f and N and corresponding wavelengths as described in Section 5.

2. Experiment

In the experiment area between 77.5°N and 79°N (Fig. 1), three buoys with thermistor chains were deployed on

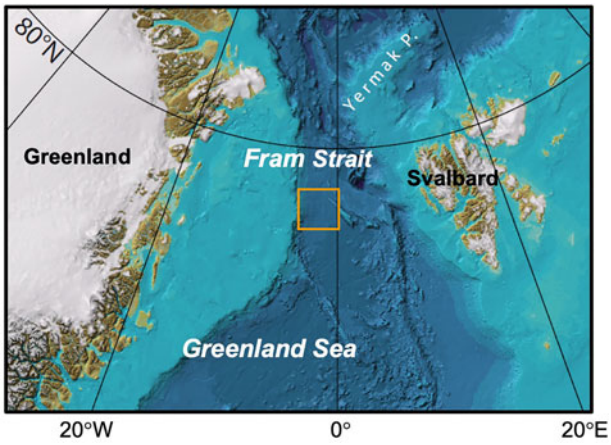

Fig. 1. Bathymetric map of the Fram Strait area and northern Greenland Sea. Yellow frame indicates the experiment area as detailed in Fig. 2a. Base map is from the International Bathymetric Chart of the Arctic Ocean (IBCAO) (Jakobsson et al. 2012).

ice floes which were a perfect platform for a drifting triangle with sides of a few km, from 30 March to 4 April 1987 (Sandven, 1988). The distance of the array to the ice edge varied between 1 and 3 km. The buoys were positioned using the Argos system (Sandven et al., 1987 1988a) with an accuracy of 250 m (http://www.argos-system.org/manual/3-location/34_location_classrs.htm). The three thermistor chains, denoted T1, T2, and T3, had sensors each 5 m between depths of 45 and 95 m, spanning the thermocline region, with 2-min sampling for temperature measurements. T1 also had current meters at 7, 15, 55, 105 and 255 m depths with 5-min sampling. From 28 March – before the internal wave experiment – to 8 April, SAR images were collected each day using two STAR aircrafts with the Intera X band (3 cm) SAR with a 12-m resolution. The SAR was optimized for ice, resulting in no imaging of the open ocean features (Shuchman et al., 1988; Johannessen et al., 1994). The SAR images were downlinked from the SAR STAR aircrafts in real time to the I/B Polar Circle which allowed us to deploy the thermistor array on the ice slightly to the west of the evolving eddy field. The oceanographic and meteorological data within the eddy field, including wind velocity at a height of 15 m above the ocean surface, were obtained from I/B *Polar Circle* and R/V *Håkon Mosby* (Sandven et al., 1987, 1988b; MIZEX '87 Group, 1989).

3. Ocean structure

The array drifted southwards inside the ice edge with a speed of 0.4–0.5 m/s, approximately 40–50 km/day, over water 2000–2400-m deep (Fig. 2a) carried by the East Greenland Current (EGC), including a contribution from the north-easterly wind during the period from 29 March to 3 April. In order to get the background of the ocean structure, the temperature and salinity versus depth were sampled on 31 March by CTD in an oceanographic section 40 km long and with station spacing of 4.4 km. The section was carried out both in the ice (indicated by a blue line in Fig. 2b,c) and in the open water perpendicular to the EGC (Fig. 2b,c). It showed that the cold Polar Water (PW) of less than –1.85 °C in the southflowing EGC was separated from the warmer Modified Atlantic Water (MAW) by the East Greenland Polar Ocean Front (Johannessen et al., 1986), where the isotherms rapidly shoaled from 100 m depth in the west to the surface in the central part of the section (Fig. 2b, where only the top 250 meters are shown). The salinity and density structures were similar and are not shown here. In this section, it is seen that the western part of the Polar Ocean front is located at the ice edge, but this will vary depending on the on- and off-ice wind direction. The estimated current computed from geostrophy, using 1000 m as the reference level, which was the deepest observational level, indicated a relative southwards flow with a speed of 0.20 m/s in the surface PW layer, while on the other side of the front in the MAW, the current was northwards with a speed of only 0.02 m/s (Fig. 2c), resulting in both horizontal and vertical shear in this frontal zone. We stress that the geostrophic current is only part of the current system (not including the barotrophic component), since the current measurement from T1 in the surface PW showed an average current speed of 0.35–0.40 m/s in a south–southwest direction during 30–31 March, although downstream from the oceanographic section (Fig. 2b,c), which was observed on 31 March. This Polar Ocean Front extends along the entire East Greenland continental slope (Johannessen et al., 1986) meandering and spinning off ice edge jets, vortex pairs, and ice-ocean eddies caused by

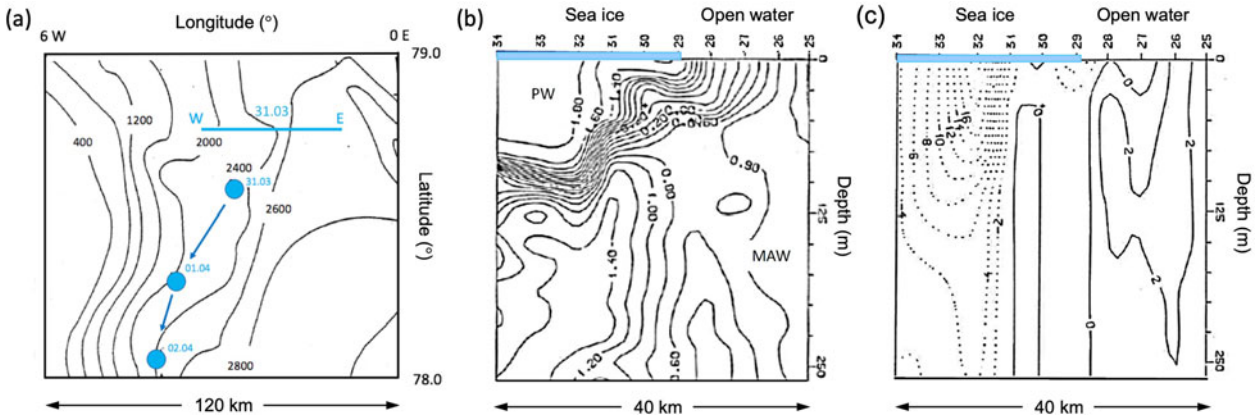

Fig. 2. a, Location and bathymetry (in metres) of the experimental area, drift of the array during 31 March – 2 April (blue dots), and oceanographic section on 31 March (blue line marked W–E). b, Temperature section across the East Greenland Sea Polar Ocean Front, PW is cold Polar Water of less than –1.8 °C; here, only the isotherms between –1.0 °C and +1.4 °C are shown for each 0.1 degree C. MAW is warm Modified Atlantic Water. c, Calculated geostrophic current in cm/s across the section with 0 reference level at 1000 m the dotted lines correspond to the southward current; full lines correspond to the northward current in cm/s contoured for each 2 cm/s from –20 cm/s to –2 cm/s southwards to 2 cm/s northwards. Sea-ice cover is shown by the thick blue line at the surface. The section is 40-km long with station spacing of 4.4 km.

baroclinic and barotropic instabilities (Johannessen et al., 1987a, 1987b).

4. Ocean eddies

On 28 March, two eddies started to develop seen as ice tongues from the main ice edge (Fig. 3b), but the signal was partly obscured, because the ice edge was compacted by a north-easterly wind of 6–8 m/s. During a calm wind period of 28–29 March with a wind speed less than 3 m/s, the SAR image mirrored the ocean circulation (Fig. 3c), indicating two clear eddies: a large anticyclonic eddy with scale of 40 km and further north a cyclonic ice edge jet ending in a vortex pair with a scale of 20 km, developed later into a cyclonic eddy (Johannessen et al., 1994). During 30 March, the north-easterly wind of 10 m/s again compacted the ice edge, obscuring part of the ice-eddies signature (Fig. 3d). On March 31, when the north-easterly wind increased up to 12 m/s, the eddies ice signatures had disappeared; however, the semi-circular pattern of the anticyclonic eddy was seen in the meandering ice edge. The ice edge on 31 March (Fig. 3e) was displaced to the west by the north-easterly wind of 12 m/s and by the orbital speed of the anticyclone moving part of the ice cover out in the warmer ocean (Fig. 3d, red arrow). The anticyclonic ocean eddy still existed on 31 March, as the eddy was evident in a north–south oceanographic CTD section, obtained on 2 April east of the ice edge, 65 km long and with station spacing of 8–11 km; the depth reached 2000 m, which was just above the bottom (Fig. 4a,b). The isolines of density were deeply depressed in the centre with Polar Water in the surface while surfacing at station 27 indicating the northern boundary of the eddy with warmer MAW to the north (Fig. 4a). The geostrophic current in the section, using the 2000 m as the reference (Fig. 4b), indicated an orbital flow, with eastwards flow of up to 0.20 m/s in the north and westwards flow of 0.10 m/s in the south in the upper layer. The schematic of this current pattern is inserted in Fig. 3e, along with a north–south velocity profile and a circular arrow. The signature of this anticyclonic eddy in the temperature, salinity (not shown), density and geostrophic flow (Fig. 4a,b), extended to the depths more than 500 m. This eddy was probably caused by instability of the East Greenland Polar Ocean Front, as supported by numerical modelling using the ocean data from the experiment to the initial model, excluding the wind (Johannessen et al., 1994). The eddy investigation in MIZEX 84 (Johannessen et al., 1987a, 1992) in the same area as in this study showed from remote sensing data that the ice floes were spinning towards the centre of these eddies, converging there, thus indicating ageostrophic effects. In this study of the anticyclone (Fig. 3c), the presence of ageostrophic effects was also established from the fact convergence of the ice in the centre of the anticyclone showing that the flow was not entirely in geostrophic balance. A theoretical study by Molemaker et al. (2010) showed that the unbalanced flow in frontal region and within mesoscale eddies, like that existed in the anticyclonic eddy, tends to generate internal waves. The latter play an essential role in the forward cascade of kinetic energy from the eddies to the small-scale turbulent motions at which this energy dissipates. However, we suggest that the most probable mechanism of generation of

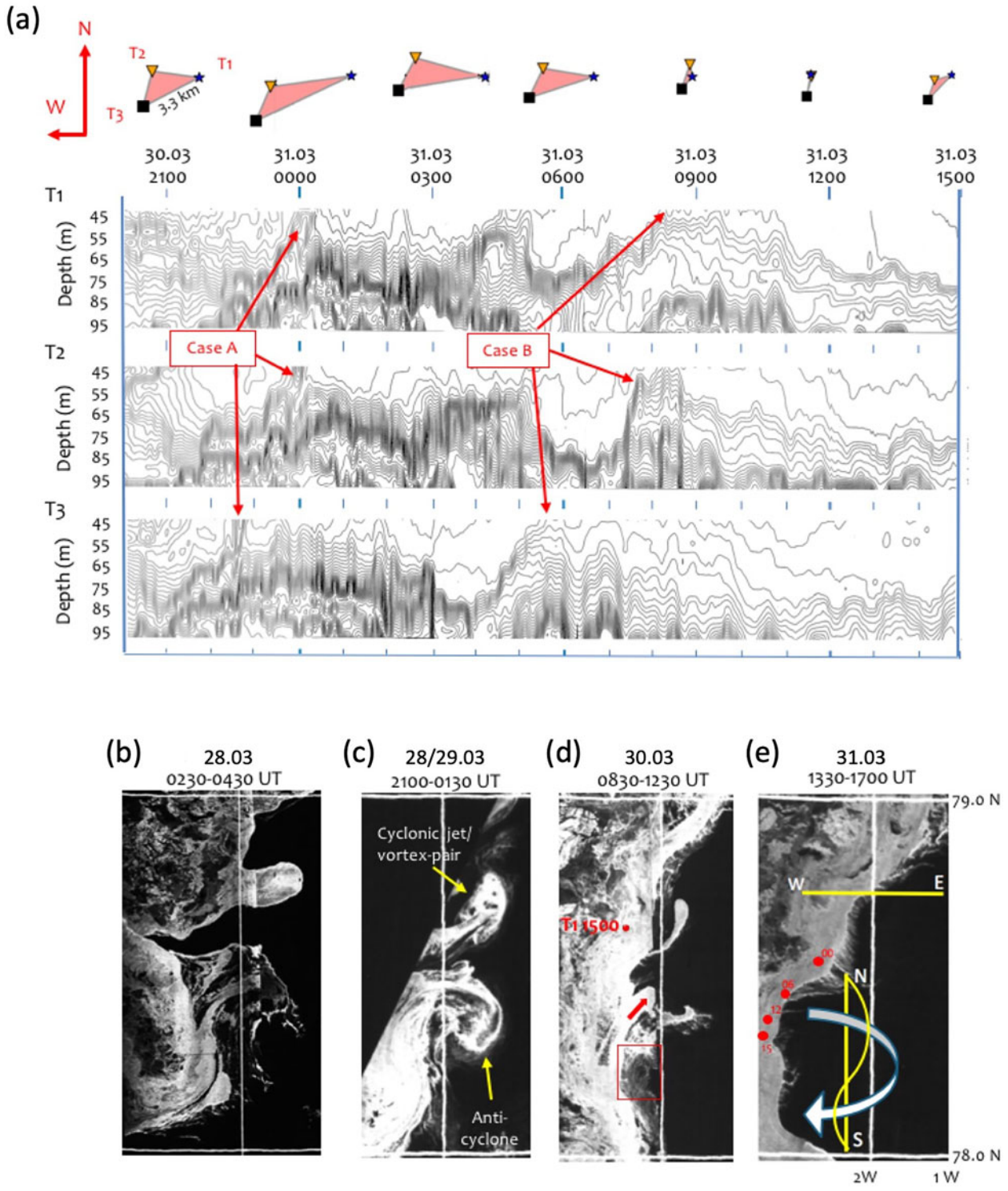

Fig. 3. Observations of internal waves and ice-ocean eddies. a, Isotherms between –1.8 °C and 1.8 °C (shown with an interval of 0.1 °C) in the thermocline layer between 45 and 95 m obtained every 2 minutes by the triangle (plotted above with 3-hour interval) with thermistor chains, spaced each 5 m. The arrival times for the two local wave crests detected during 30–31 March are marked as Case A and Case B. b–e, Synthetic Aperture Radar (SAR) images from 28–31 March. Red dot marks the deployment of the array on 30 March, and red arrow indicates the flow of the ice in the anticyclonic eddy; the red box shows the area where the internal waves are observed (see Fig. 3a). Red dots in E show the array on 31 March at 00:00, 06:00, 12:00 and 15:00. Yellow lines are the East (E)–West (W) oceanographic section obtained on 31 March (in Fig. 2b,c) and the North (N)–South (S) section obtained on 2 April. Schematically, the E–W geostrophic profile is shown by a curved yellow line and the circular white arrow shows the anticyclonic eddy. See Fig. 4.

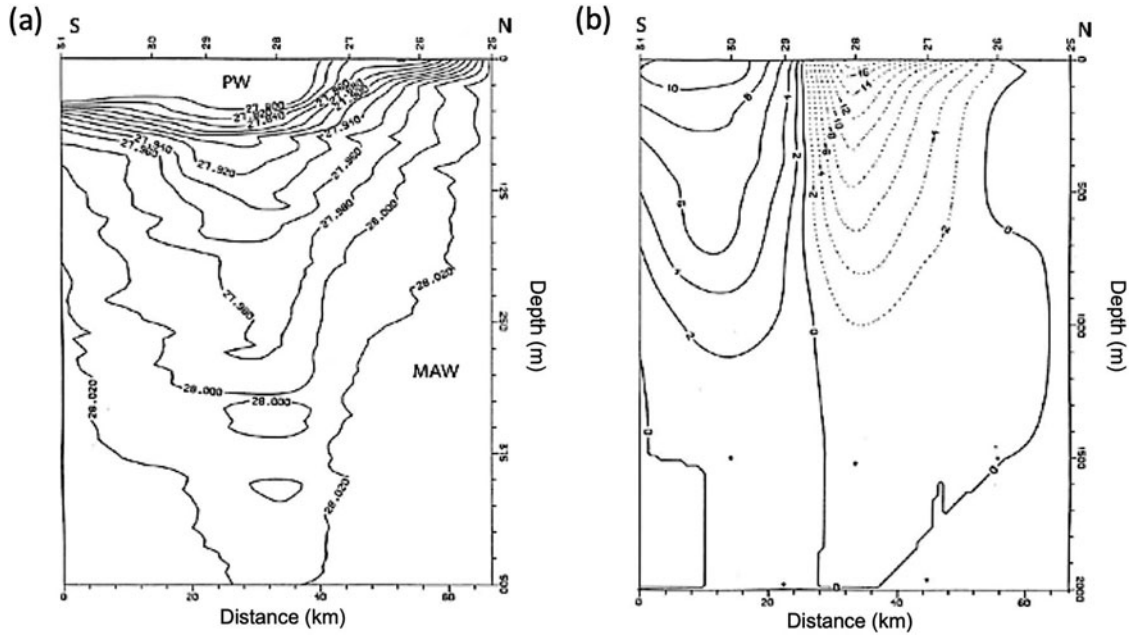

Fig. 4. The anticyclonic eddy characteristics. a, Density section of the North (N)–South (S) section on 2 April shown in Fig. 3e. b, Geostrophic current in the N–S section with 0 reference level at 2000 m. Dotted lines: eastward current; full lines: westward current in cm/s. Note the different y-axis scale for the depth, 500 m for a and 2000 m for b. The section is 65-km long and with station spacing of 8–11 km.

the observed internal waves is described in detail by the theory of Plougonven and Zeitlin (2002), as mentioned in the Introduction.

5. Internal waves

Internal waves were observed when the array drifted in a south–south-west direction in the Polar Water (Fig. 2a) west of the anticyclone (Fig. 3e). The isotherms (Fig. 3a) covered a range from –1.8 °C in the surface layer to +1.8 °C in the deeper part of the thermocline. The internal wave frequencies relative to the triangle were in the range 1–3 cycles per hour (cph), which is between the buoyancy frequency (N) of 6.5 cph, calculated from a density profile (station 34 in Fig. 2b), and the inertial frequency of about 0.08 cph, which is the same as the semidiurnal frequency for this latitude. The lower frequency variations in the isotherm displacements with periods of 4–5 hours were likely caused by meandering of the thermocline of the Polar Ocean Front (Fig. 2b) when the array drifted downstream in a south–south-west direction (Fig. 2a). The measured semidiurnal tidal current from T1 was a few cm/s, which is approximately 10% of the observed average current speed. The background MIZEX 87 vertical displacement spectrum of the internal waves in the thermocline (m^2/cph) for the whole observational period from March 30 to April 4 (Fig. 5) was calculated from the thermistor chain T1, based on the temperature variation at 60 m divided by a mean temperature gradient of 0.10 °C/m because some of the isotherms were discontinuous. The spectrum had the same slope as the Garrett–Munk (GM) spectrum (Garrett and Munk, 1972, 1975) for the global ocean. However, the spectral level was 2–3 times less than that for GM spectrum and similar to the spectrum calculated previously during the MIZEX 83 Internal Wave Experiment north of Svalbard in the ice edge region (Sandven and Johannessen, 1987), but subjected to Doppler shift towards higher frequencies (see below in Section 6). Both semidiurnal and inertial frequencies that were roughly the same at this latitude showed a weak peak in the spectrum indicating that internal waves at this frequency were not dominant. The reason for the lower spectral level in the Arctic region compared with the open ocean is not fully understood, but Levine et al. (1985) suggested that the ice cover dampens internal waves via a turbulent boundary layer and that the internal wave generation also depends on the underside roughness and topography of the ice cover (Morison, 1986). Furthermore, wind and internal tides are generally weaker in the Arctic Ocean compared to the global ocean, as treated in more detail by Levine et al. (1987).

Importantly, internal waves were also observed in the SAR image of March 30 (Fig. 6a) in the western part of

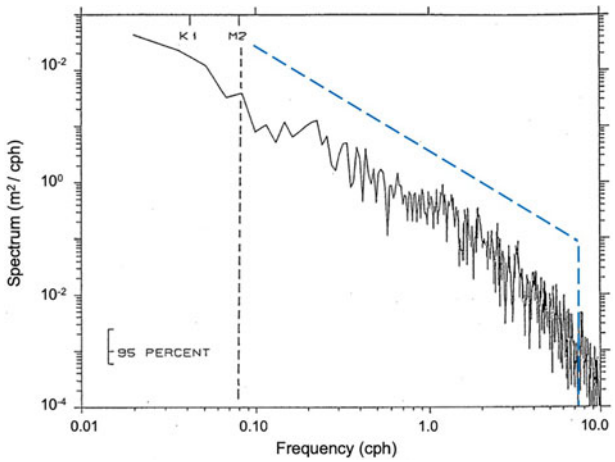

Fig. 5. The vertical displacement spectrum computed from 30 March to 4 April of the temperature series from the thermistor T1 at 60 m, divided by the mean vertical temperature gradient of 0.10 degree C/m is compared to the Garrett-Munk spectrum, shown by the dotted line. The inertial period is close to the semidiurnal period for this latitude and the cut-off buoyancy frequency (N) is 6.5 cph. The spectrum is estimated by fast Fourier transformation (FFT), and the 95% confidence level is based on 10% tapering of the series and smoothing over five frequency bands with a resolution of 0.02 cph (Bloomfield,1976). The Garrett-Munk spectrum is plotted using a scaling factor $R = 320$ (exponent 2) cph and a cut-off frequency $N = 6.5$ cph (See Sandven and Johannessen (1987) for more details).

the anticyclone east of the drifting array. The internal wave signatures on the surface appear as curved slicks of ice bands with wavelengths of 750–1000 m at the western boundary of the anticyclone. The ice slicks were caused by the regular convergence and divergence of the surface current of the internal wave field (Eckart, 1961; La Fond, 1962). It is seen that the internal wavefronts are slightly curved and cylindrically diverging from the area occupied by the western part of the anticyclonic eddy (Fig. 6a). We interpret them as internal waves propagating westwards away from the anticyclone, indicating that this anticyclonic eddy was the source of the internal waves detected by the drifting thermistor array as was confirmed by the analysis of their characteristics (see Sections 6 and 7). We further argue that the observed internal waves cannot originate from the nearby homogeneous MAW in the deep basin east of the anticyclone, since the buoyancy frequency N there is less than the frequency N we observed.

6. Analysis

Because our internal wave observations were from a drifting array with velocity close to the mean current velocity $\vec{V}_0$ in the thermocline region, the intrinsic angular frequency, $\omega = \omega_0 - k_x V_{0,x} - k_y V_{0,y}$ of the observed internal waves, was Doppler-shifted with respect to the frequency ω_0 relative to the ground. Here, k_x and k_y are the components of the horizontal wavenumber vector $\vec{k}_\perp$, while $V_{0,x}$ and $V_{0,y}$ are the components of the current velocity $\vec{V}_0$. Knowing the current velocity measured at T1 we can estimate a Doppler-shift $\vec{k}_\perp \cdot \vec{V}_0$ of the frequency.

We will focus on the internal waves with intrinsic linear frequencies $f = \omega/(2\pi)$ of 1–3 cph that were observed during 30–31 March when the array drifted southwards, close to the ice edge, and west of the anticyclonic eddy (Fig. 3d,e). For low frequencies, $\omega^2/N^2 \ll 1$, where $N = 6.5$ cph (as calculated from station 34 in Fig. 2a), the dispersion relation for internal wave modes under hydrostatic approximation is given by $\omega \approx N \cdot k_\perp/m$ (Gill, 1982), where m is vertical wavenumber. In this case, the intrinsic group velocity of the wave train $\vec{C}_g = \partial\omega/\partial\vec{k}_\perp = (N/m) \cdot \vec{k}_\perp/k_\perp$ is directed in the same direction as $\vec{k}_\perp$ and it coincides with the horizontal phase speed $\omega/k_\perp = N/m$. The latter does not depend on $k_\perp$ or horizontal wavelength $\lambda = 2\pi/k_\perp$. Because the wave train is advected by the current, its absolute group velocity $\vec{C}_{g0} = \partial\omega_0/\partial\vec{k}_\perp$ relative to the ground is $\vec{C}_{g0} = \vec{C}_g + \vec{V}_0$.

When the array drifted southwards and west of the anticyclone, we choose two different local wave crests within the observed long-lasting wave train to estimate its local phase and group velocities. The first wave crest, indicated as Case A in Fig. 3a, was detected by T3 at 22:40 on 30 March, with dominant intrinsic frequency of 3 cph, and the second wave crest, Case B, was detected at 05:40 on 31 March with dominant intrinsic frequency of 1 cph (Fig. 3a).

Case A was also detected by T2 and T1 at 00:00 on 31 March, with internal wave amplitudes of 3–15 m. Using the triangle position at 00:00 on 31 March and the time delays between T1, T2 and T3, the calculated intrinsic group speed (the same as the phase speed) was about 0.34 m/s, with an accuracy of 20% based on the Argos

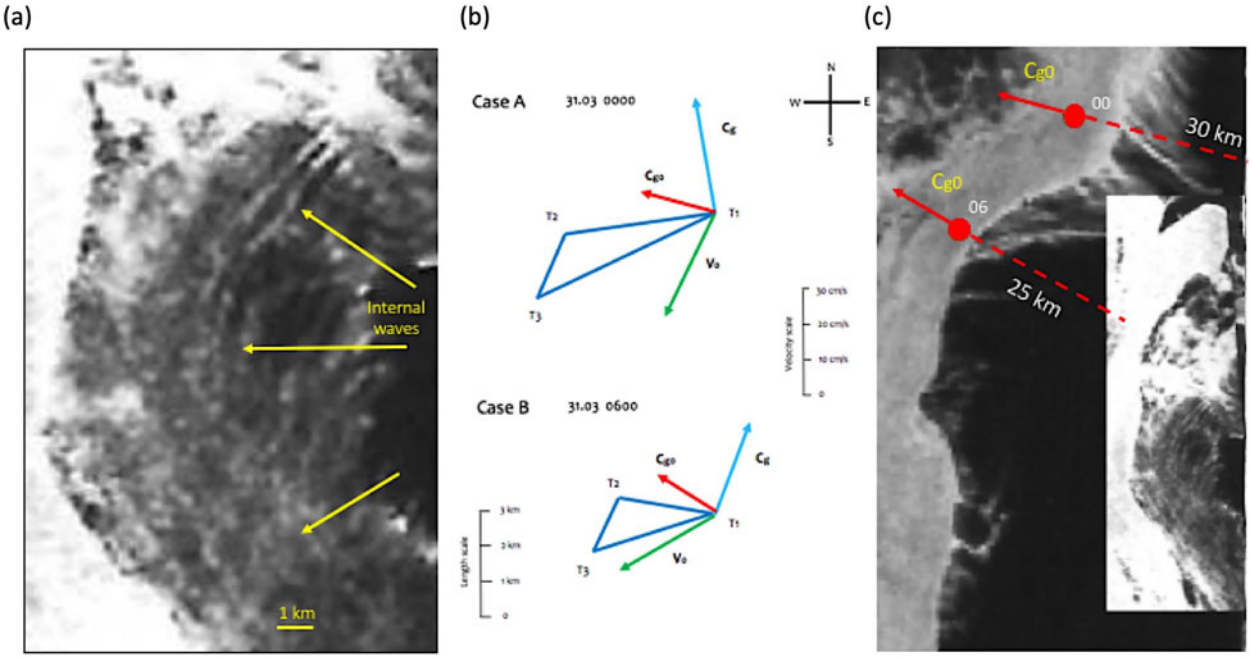

Fig. 6. Imagery of internal waves and velocity calculations. a, Synthetic Aperture Radar (SAR) image of internal wave train with the wavelengths of 750–1000 m propagating at the western boundary of the anticyclone eddy (shown for 30 March by the slicks of curving bands of ice floes); for the location see red box in Fig. 3d. b, The triangle array T1-T2-T3 at 00:00 and 06:00 of 31 March, $\vec{C}_g$ is the intrinsic group velocity of the internal wave train, $\vec{V}_0$ is the average current velocity in the thermocline region, $\vec{C}_{g,0}$ is the absolute group velocity relative to the ground. c, SAR image of 31 March. Red dots are the array positions at times 00 and 06 shown along with the absolute group velocity vectors, $\vec{C}_{g,0}$. Inserted is the part of the SAR image from 30 March, which includes the box shown in Fig. 3d. Dotted red lines from the array positions are backward extrapolation directions of the absolute group velocities hitting the internal waves on 30 March.

position error of 250 m, and a wavelength of 400 m. The group velocity relative to the drifting triangle array, $\vec{C}_g$, the absolute group velocity relative to the ground, $\vec{C}_{g,0}$, and the average current velocity $\vec{V}_0$ in the thermocline region are plotted in Fig. 6b. Since the average current speed in the thermocline region $V_0 \approx 0.3$ m/s, and the angle ϕ between vector $\vec{V}_0$ and wavenumber vector $\vec{k}_\perp$ was close to 145°, the Doppler shift $\Delta f = V_0 \cos\phi/\lambda$ was about –0.72 cph, hence the frequency with respect to the ground $f_0 = f + \Delta f \approx 2.3$ cph. The estimated absolute group velocity $C_{g,0} \approx 0.24$ m/s directed towards 286° shows that the internal wave train propagated westwards away from the anticyclonic eddy (Fig. 6a–c) .

In Case B, the internal wave crest was detected by T3 at 05:40, by T2 at 07:30 and by T1 at 08:00 of March 31. The dominant wave intrinsic frequency f was about 1 cph; hence, the group velocity C_g of the waves was about 0.27 m/s with a wavelength λ of 970 m based on the position of the triangle at 06:00 shown in Fig. 3a. This wavelength is in a good agreement with the wavelength of 750–1000 m observed in the SAR image (Fig. 6a). The plot (Fig. 6b) of the vectors $\vec{C}_g$, $\vec{V}_0$ and $\vec{C}_{g,0}$ gave the values 0.24, 0.30 and 0.17 m/s, respectively, showed again that the internal waves propagated westwards, but with slightly greater northwards component than that for the Case A. Since the angle ϕ was about 140°, and the average velocity $V_0 \approx 0.3$ m/s, the Doppler shift $\Delta f = V_0 \cos\phi/\lambda$ was about –0.85 cph, therefore the frequency with respect to the ground, $f_0 = f + \Delta f = 0.15$ cph.

For the Case A, the group velocity vector $\vec{C}_{g,0}$ was extrapolated backwards, where the part of the image obtained the day before is inserted (Fig. 6c). The extrapolated line indicates the back azimuth of the internal wave source and shows that the internal wave energy arrives from the finite area occupied by the northern part of the anticyclonic eddy, which is roughly 30 km away the array.

For the Case B, the back azimuth direction of $\vec{C}_{g,0}$ of the extrapolated line shows that the internal wave energy propagates from the centre of the anticyclone (Fig. 6c). The distance between the triangle and the internal waves observed in the SAR image, obtained the day before, was about 25 km (Fig. 6c).

Thus, in both cases A and B, the internal wave energy arrives from the local area occupied by anticyclonic eddy. This fact is consistent with the mechanism of permanent

radiation of internal waves by the non-stationary vortex motions with some distribution of potential vorticity within a finite area of the ocean (Plougonven and Zeitlin, 2002 and references therein). It is important to note that SAR imaged the evolution of the anticyclone vortex (Fig. 3b–e) in the time period during which we observed a long-lasting internal wave train shown in Fig. 3a. The amplitude of the isotherm displacements caused by the internal wave train started to increase with time in the night of March 30 and gradually decreased by 15:00 of 31 March. Also, the density of the distribution of isotherms and local gradients in temperature essentially increased during mentioned period which means that the internal wave field was essentially nonlinear within the wave train and had a wide frequency spectrum localized between f and N. The estimated back azimuths of the wave crests of the wave train indicated that internal wave energy arrives to the drifting array from the observed anticyclonic eddy.

7. Discussion

Our findings have indicated that the two local internal wave crests of the entire wave train, cases A and B, detected by the ice drifting array were radiating from the evolving anticyclonic eddy located east of the array. This is consistent with the theory by Plougonven and Zeitlin (2002) which predicted a cylindrical divergence of internal wave field from an evolving eddy. The current flow and pressure within the eddy depend on time, because according to this theory 'the nonlinearity of the vortex motion removes it from the state of quasistatic and cyclostrophic equilibrium, which is accompanied by emission of internal waves'. From the SAR images in Fig. 3b–e, we see that the eddy indeed evolves in time. Moreover, from the frequency spectrum (Fig. 5), we assume that the anticyclone's current is turbulent in nature and contains temporal and spatial fluctuations of velocity and pressure. Furthermore, the Plougonven and Zeitlin's (2002) theory predicts cylindrical divergence of the internal wave field from the eddy. This theoretical prediction is also confirmed by the SAR image (Fig. 6a) with the curved wave crests propagating from the western part of the anticyclonic eddy into the ice cover.

According to the Plougonven and Zeitlin's (2002) theory, we also expect that internal waves propagate radially to the areas around the eddy, but unfortunately, we do not have any internal wave observations in the open ocean to the east of the anticyclonic eddy to confirm this. However, our expectation is supported by Sandven and Johannessen (1987, their Fig. 1) which indicated that a small eddy generated internal waves which were cylindrically diverging waves from the eddy, as mentioned in the Introduction.

The wavelengths of the internal waves (750–1000 m) clearly imaged by SAR (Fig. 6a), were in agreement with those calculated from the drifting array (see Case B). We also estimated phase and group velocities of the local internal wave crests of the observed wave train. Using these estimates we found that the internal wave energy arrives from the sources whose back azimuths coincide with the different parts of the anticyclonic vortex. This fact was consistent with the generation mechanism of internal waves by the non-stationary vortex motions (Plougonven and Zeitlin, 2002) with some distribution of vorticity over a finite area of the ocean occupied by the anticyclonic vortex. The estimated back azimuths of different parts of the entire radiating vortex depend on the location of drifting array and the current velocity vector during the period of evolution in time of the anticyclonic eddy imaged by SAR, Fig. 3b–e.

The array was drifting inside the ice edge (Fig. 3d,e), which coincides with the eastern part of the Polar Ocean Front (Fig. 2b). Internal waves could also be generated by destabilization of this front with the same range of frequencies as for any other sources, including eddies and underside ice ridges. We suggest, however that the source of the observed internal waves is indeed the anticyclonic eddy based on the five following arguments: (1) The time period from the 28 March to midday of 31 March where the anticyclonic eddy evolved in time, shown by the SAR images in Fig. 3b–e, coincided with the internal wave train direction from the evening of 30 March with increasing amplitude of the isotherm oscillations and decreasing amplitude by 12.00 on 31 March, Fig. 3a. Also, the density of the distribution of isotherms and local vertical gradients in temperature increased during the period as compared to the period before the evening of 30 March, which means that the internal wave field within the wave train was essentially nonlinear and had a wide frequency spectrum between f and N, consistent with the Plougonven and Zeitlin's (2002) theory. As the array was drifting southwards, the back azimuths of the direction of the group velocity of the wave train at different times (Fig. 6b,d) showed that the wave energy was coming from a finite area occupied by the anticyclonic eddy (Fig. 6a). Importantly, the SAR image of 30 March (Fig. 6a) also showed surface internal wave signatures that appear as curved slicks of ice band with wavelengths of 750–1000 m which cylindrically diverged from the area occupied by the eddy, again supporting conclusion that the anticyclonic eddy was the major source for the observed internal waves associated with the crests A and B. (2) A destabilization of the Polar Ocean Front could also generate internal waves. However, the frontal

geometry stretching all along the Greenland Sea does not correspond to the internal diverging wave crests observed in the SAR image in the western part of the anticyclone, Fig. 6a. We conclude therefore that the Polar Ocean Front is not the major source for the internal wave trains, A and B. Nonetheless, the Polar Ocean Front observed (Fig. 2b,c) is important for generating eddies through baroclinic and barotrophic instability mechanisms as shown by Johannessen et al. (1994) for the MIZEX 87 experiment. (3) Since the back azimuth of the group velocity of the internal wave crests, A and B, can be tracked back to the anticyclonic, we conclude that the underwater ice ridges cannot be the source for the internal wave trains (A and B). Furthermore, we expect according to the Plougonven and Zeitlin's (2002) theory that eddies generate internal waves with a wide range of frequencies and wavelengths due to the proposed generation mechanism of internal waves caused by temporal current and pressure variations inside the eddy. This mechanism exists regardless of the existence of ice. However, the ice cover was important as a convenient platform for the thermistor array and the current meter string from T1. (4) As mentioned before, we argue that the observed internal waves cannot originate from the nearby homogeneous MAW in the deep basin east of the anticyclone, since the buoyancy frequency N there is less than the frequency N that we observed. (5) Furthermore, no directional internal waves were imaged by the SAR or detected by the thermistor array when it passed west of the jet vortex pair observed north of the anticyclonic eddy, and only background internal waves before Case A were found (Fig. 3a–e), again supporting our conclusion that the source of internal waves was the anticyclonic eddy.

From these five points and other results of our observations and analysis described previously, we conclude that the temporally evolving anticyclonic eddy was the main source of the observed internal wave train, A and B, among other permanently existing background sources of internal waves such as wind flow over ocean and ice surfaces, destabilization of the Polar Ocean Front or topographically generated by the rough underside of the ice-by-ice ridges, as observed in the Arctic Ocean (Morison, 1986).

According to Plougonven and Zeitlin (2002) theory, vortexes or eddies should in principal be able to generate internal waves, but whether this is the case or partly the case remains an open question. Sandven and Johannessen's (1987) paper indicated a small eddy which generated radial propagating internal waves, and in this paper, we have seen that an anticyclonic eddy can generate internal waves from part of the eddy. On the other hand, the jet vortex pair north of the anticyclone appeared not to generate directional internal waves. Therefore, it is an open and interesting question to investigate the importance of eddy fields as new sources of generating internal waves in the global ocean.

8. Conclusions

We conclude that the main source for the internal waves observed in Cases A and B was the anticyclonic eddy. Therefore, our case study suggests that ocean eddies can possibly be the direct sources of internal wave generation, as observed here for the first time, and not only enhance the local internal waves by draining energy from eddies (Clément et al., 2016). Since mesoscale eddies are abundant in all coastal and ocean areas, this hypothesis should be further tested by theoretical studies and dedicated field experiments in eddy regions to see how important this is. In general, SAR can image both internal waves (Alpers and Salusti, 1983) and eddies (Johannessen et al., 1996) under moderate wind conditions; therefore, a way to start is to analyse the vast numbers of SAR images available for the global coastal regions and World Oceans and to search for eddies to see whether internal waves are generated by them, before field experiments are done – a challenge for the future.

Acknowledgements

The authors thank the late Walter Munk for comments to a preliminary draft of this paper and Carl Wunch for useful comments on the present paper. We also thank the two anonymous reviewers for useful comments that improved the paper. Brian Dushaw and Martin Miles are acknowledged for editing the paper.

Disclosure statement

No potential conflict of interest was reported by the authors.

Funding

The MIZEX '87 program was supported by research councils, universities and institutes of the participating nations (Norway, USA), including Johnny A. Johannessen from the Nansen Center in Bergen, who was the Chief Scientist on R/V *Håkon Mosby*. This research was also partially supported by grants RFBR №16-05-00438, 18-55-05002, RSF 14-47-00049 (Russia).

References

Alford, M. H. 2003. Redistribution of energy available for ocean mixing by long-range propagation of internal waves. *Nature* **243**, 159–163.

Alpers, W. and Salusti, E. 1983. Scylla and Charybdis observed from space. *J. Geophys. Res.* **88**, 1800–1808. doi:10.1029/JC088iC03p01800

Barkan, R., Winters, K. B. and McWilliams, J. C. 2017. Stimulated imbalance and the enhancement of eddy kinetic energy dissipation by internal waves. *J. Phys. Oceanogr.* **47**, 181. doi:10.1175/JPO-D-16-0117.1

Bloomfield, P. 1976. *Fourier Analysis of Time Series, an Introduction*. John Wiley, New York.

Chunchuzov, I. P. 2018. Nonlinear formation of the three-dimensional spectrum of mesoscale wind velocity and temperature fluctuations in stably stratified atmosphere. *J. Atmos. Sci.* **75**, 3447–3467. doi:10.1175/JAS-D-17-0398.1

Clément, L., Frajka-Williams, E., Sheen, K. L., Brearley, J. A. and Garabato, A. C. N. 2016. Generation of internal waves by eddies impinging on the Western Boundary of the North Atlantic. *J. Phys. Oceanogr.* **46**, 1067–1079. doi:10.1175/JPO-D-14-0241.1

Eckart, C. 1961. Internal waves in the ocean. *Phys. Fluids* **4**, 791–799. doi:10.1063/1.1706408

Garrett, C. J. R. and Munk, W. H. 1972. Space-time scales of internal waves. *Geophys. Fluid Dyn.* **2**, 225–264.

Garrett, C. J. R. and Munk, W. H. 1975. Space-time scales of internal waves: A progress report. *J. Geophys. Res.* **80**, 291–297. doi:10.1029/JC080i003p00291

Gill, A. E. 1982. *Atmosphere-Ocean Dynamics*, Vol. 30. Academic Press, New York, pp. 159–162.

Jakobsson, M., Mayer, L., Coakley, B., Dowdeswell, J. A., Forbes, S. and co-authors. 2012. The International Bathymetric Chart of the Arctic Ocean (IBCAO) Version 3.0. *Geophys. Res. Lett.* **39**, n/a–6.

Johannessen, J. A., Shuchman, R. A., Digranes, G., Lyzenga, D. R., Wackerman, C. and co-authors. 1996. Coastal ocean fronts and eddies imaged with ERS 1 synthetic aperture radar. *J. Geophys. Res.* **101**, 6651–6667. doi:10.1029/95JC02962

Johannessen, O. M., Johannessen, J., Sandven, S., Davidson, K. L. 1986. Preliminary results of the marginal ice zone experiment (MIZEX) summer operations. In: *The Nordic Seas* (ed. B. G. Hurdle), Springer Verlag, New York, 666–679 pp.

Johannessen, O. M., Johannessen, J. A., Svendsen, E., Shuchman, R. A., Campbell, W. J. and co-authors. 1987. Ice-edge eddies in the Fram Strait marginal ice zone. *Science* **236**, 427–429. doi:10.1126/science.236.4800.427

Johannessen, J. A., Johannessen, O. M., Svendsen, E., Shuchman, R., Manley, T. and co-authors. 1987. Mesoscale eddies in the Fram Strait Marginal Ice Zone during the 1983 and 1984 Marginal Ice Zone Experiment. *J. Geophys. Res.* **92**, 6754–6772. doi:10.1029/JC092iC07p06754

Johannessen, O. M., Sandven, S., Budgeu, W. P., and Johannessen, J. A. 1994. Observation and simulation of ice tongues and vortex pairs in the marginal ice zone. In: *The Polar Oceans and Their Role in Shaping the Global Environment, the Nansen Centennial Volume* (eds. O. M. Johannessen. et al.) Vol. **85,** Geophysical Monograph, American Geophysical Union, Washington, D.C., pp. 109–136.

Johannessen, O. M. 1986. Brief overview of the physical oceanography. In: *The Nordic Seas* (ed. B. G. Hurdle), Springer Verlag, New York, pp. 103–127.

Johannessen, O. M., Campbell, W. J., Shuchman, R., Sandven, S., Gloersen, P. and co-authors. 1992. Microwave study programs of air-ice-ocean interactive processes in the seasonal ice zone of the Greenland and Barents seas. Ch. 13, 261–289. In: *Microwave Remote Sensing of Sea Ice* (ed. F. Carsey) Vol. 68, Geophysical Monograph, American Geophysical Union, Washington, D.C.

Krauss, W. 1999. Internal tides resulting from the passage of surface tides through and eddy field. *J. Geophys. Res.* **104**, 18323–18331. doi:10.1029/1999JC900067

La Fond, E. C. 1962. *The Sea* (ed. M. N. Hill), Wiley Interscience, New York, pp. 731–751.

Lelong, M. P. and Riley, J. J. 1991. Internal wave–vortical mode interactions in strongly stratified flows. *J. Fluid Mech.* **232**, 1–19. doi:10.1017/S0022112091003609

Levine, M. D., Paulson, C. A. and Morison, J. H. 1985. Internal waves in the Arctic Ocean: Comparison with lower latitude observations. *J. Phys. Oceanogr.* **15**, 800–809. doi:10.1175/1520-0485(1985)015<0800:IWITAO>2.0.CO;2

Levine, M. D., Paulson, C. A. and Morison, J. H. 1987. Observations of internal gravity waves under the Arctic pack ice. *J. Geophys. Res.* **92**, 779–782. doi:10.1029/JC092iC01p00779

Lighthill, J. M. 1952. On sound generated aerodynamically. I. General theory. *Proc. R. Soc. London, Ser. A* **211**, 564.

Miropolsky, Y. Z. 2001. *Dynamics of the Internal Gravity Waves in the Ocean*. Springer-Science + Business Media B. V., Dordrecht, Netherlands.

MIZEX '87 Group. 1989. MIZEX 1987. Winter marginal ice zone program in the Fram Strait and Greenland Sea. *EOS Transactions* **70**, 545–555.

Molemaker, J., McWilliams, J. C. and Capet, X. 2010. Balanced and unbalanced routes to dissipation in an equilibrated Eady flow. *J. Fluid Mech.* **654**, 35–63. doi:10.1017/S0022112009993272

Morison, J. H. 1986. Internal waves in the Arctic Ocean: A review. In: *Geophysics of Sea Ice* (ed. N. Untersteiner), Plenum, New York, pp. 1163–1183.

Munk, W. 1981. Internal waves and small scale processes. In: *Evolution of Physical Oceanography Scientific Surveys in Honor of Henry Stommel* (eds. B. A. Warren and C. Wunsch), The MIT Press, Cambridge, pp. 264–291.

Phillips, O. M. 1967. Theoretical and experimental study of gravity wave interactions. In: *Proc. of the Royal Soc.: a Discussion on Nonlinear Theory of Wave Propagation in Dispersive System, Org* (ed. M. J. Lighthill) Vol. **299.** Series A Math. And Phys. Sci., London, pp. 141–160.

Pinkel, R. 2008. Advection, phase distortion, and the frequency spectrum of finescale fields in the sea. *J. Phys. Oceanogr.* **38**, 291–313. doi:10.1175/2007JPO3559.1

Plougonven, R. and Zeitlin, V. 2002. Internal gravity wave emission from a pancake vortex: An example of wave vortex interaction in strongly stratified flows. *Phys. Fluids* **14**, 1259–1268. doi:10.1063/1.1448297

Sandven, S. 1988. *Temperature Measurement during MIZEX 87*. Technical Report No. 18, Nansen Remote Sensing Center, Bergen, Norway.

Sandven S., Geiger, C., Johannessen, J. A. and Johannessen, O. M. 1987. CTD data report from Håkon Mosby during Winter MIZEX March–April 1987, Technical Report No. 3, Nansen Remote Sensing Center, Bergen, Norway.

Sandven, S. and Johannessen, O. M. 1987. High-frequency internal wave observations in the marginal ice zone. *J. Geophys. Res.* **92**, 6911–6920. doi:10.1029/JC092iC07p06911

Sandven, S., Pettersson, L. H., Samuel, P., Johannessen, O. M. and Olaussen, T. I. 1988a. *MIZEX'87: Argos Buoy and Current Measurements*. Technical Report No. 11, Nansen Remote Sensing Center, Bergen, Norway.

Sandven, S., Kovacs, Z., Geiger, C., Olaussen, T. I. and Johannessen, O. M. 1988b. *MIZEX'87: CTD Data Report from Polar Circle*. Technical Report No. 13, Nansen Remote Sensing Center, Bergen, Norway.

Shuchman, R. A., Sutherland, L. L. and Johannessen, O. M. 1988. Geophysical information on the winter marginal ice zone obtained from SAR. In: *Proceedings of IGARSS'88 Symposium, International Geoscience and Remote Sensing Symposium*, Edinburgh, Scotland, 1988. Remote Sensing: Moving Toward the 21st Century. Vol. 2, 1111–1114,

Wunsch, C. and Ferrari, R. 2004. Vertical mixing, energy, and the general circulation of the oceans. *Ann. Rev. Fluid Mech.* **36**, 281–314. doi:10.1146/annurev.fluid.36.050802.122121